1521-0103/373/3/353–360$35.00
THE JOURNAL OF PHARMACOLOGY AND EXPERIMENTAL THERAPEUTICS

https://doi.org/10.1124/jpet.119.263772
J Pharmacol Exp Ther 373:353–360, June 2020

The Journal of PHARMACOLOGY And Experimental Therapeutics

Development of an In Vivo Method to Estimate Effective Drug Doses and Quantify Fatty Acid Amide Hydrolase in Rodent Brain using Positron Emission Tomography Tracer [^{11}C]DFMC[S]

Tomoteru Yamasaki, Tomoyuki Ohya, Wakana Mori, Yiding Zhang, Hidekatsu Wakizaka, Nobuki Nengaki, Masayuki Fujinaga, Tatsuya Kikuchi, and Ming-Rong Zhang

Department of Advanced Nuclear Medicine Sciences, National Institute of Radiological Sciences, Quantum Medical Science Directorate, National Institutes for Quantum and Radiological Science and Technology, Chiba, Japan (T.Y., T.O., W.M., Y.Z., H.W., N.N., M.F., T.K., M.-R.Z.) and SHI Accelerator Service Co. Ltd, Tokyo, Japan (N.N.)

Received November 6, 2019; accepted March 27, 2020

ABSTRACT

Fatty acid amide hydrolase (FAAH) is a key enzyme in the endocannabinoid system. *N*-(3,4-Dimethylisoxazol-5-yl)piperazine-4-[4-(2-fluoro-4-[^{11}C]methylphenyl)thiazol-2-yl]-1-carboxamide ([^{11}C]DFMC) was developed as an irreversible-type positron emission tomography (PET) tracer for FAAH. Here, we attempted to noninvasively estimate rate constant k_3 (rate of transfer to the specifically-bound compartment) as a direct index for FAAH in the rat brain. First, the two-tissue compartment model analysis including three parameters [K_1-k_3, two-tissue compartment model for the irreversible-type radiotracer (2TCMi)] in PET study with [^{11}C]DFMC was conducted, which provided 0.21 ± 0.04 ml·cm^{-3}·min^{-1} of the net uptake value (K_i), an indirect index for FAAH, in the FAAH-richest region (the cingulate cortex). Subsequently, to noninvasively estimate K_i value, the reference model analysis (Patlak graphical analysis reference model) was tried using a time-activity curve of the spinal cord. In that result, the noninvasive K_i value (K^{REF}) was concisely estimated with high correlation ($r > 0.95$) to K_i values based on 2TCMi. Using estimated K^{REF} value, we tried to obtain calculated-k_3 based on previously defined equations. The calculated k_3 was successfully estimated with high correlation ($r = 0.95$) to direct k_3 in 2TCMi. Finally, the dose relationship study using calculated k_3 demonstrated that in vivo ED_{50} value of [3-(3-carbamoylphenyl)phenyl] *N*-cyclohexylcarbamate, a major inhibitor of FAAH, was 66.4 μg/kg in rat brain. In conclusion, we proposed the calculated k_3 as an alternative index corresponding to regional FAAH concentrations and suggested that PET with [^{11}C]DFMC enables occupancy study for new pharmaceuticals targeting FAAH.

SIGNIFICANCE STATEMENT

In the present study, we proposed calculated k_3 as an alternative index corresponding with fatty acid amide hydrolase concentration. By using calculated k_3, in vivo ED_{50} of [3-(3-carbamoylphenyl)phenyl] *N*-cyclohexylcarbamate was successfully estimated to be 66.4 μg/kg for rats. Thus, we demonstrated the pharmacological utility of positron emission tomography with *N*-(3,4-dimethylisoxazol-5-yl)piperazine-4-[4-(2-fluoro-4-[^{11}C]methylphenyl)thiazol-2-yl]-1-carboxamide.

Introduction

The endocannabinoid system is known as a key biologic system having retrograde neurotransmission in the central nervous system (Devane et al., 1992; Bayewitch et al., 1995) and has been reported to regulate a broad range of physiologic processes in multiple disorders, such as pain, neuroinflammation, anxiety, neurodegenerative disorders, cancer, epilepsy, and metabolic syndrome (Pacher et al., 2006). Endocannabinoids (anandamide and 2-arachidonoyl glycerol) are synthesized by several enzymes, depending on the intracellular Ca^{2+} concentration, on postsynaptic neurons and metabolized by fatty acid amide hydrolase (FAAH) and monoacylglycerol lipase (Piomelli, 2003; Ahn et al., 2008). Among the endocannabinoids, anandamide has important roles for the activation of microglia in neuroinflammation (Raboune et al., 2014; Malek et al., 2015). Moreover, a great deal of evidence from preclinical studies indicates that elevating anandamide concentrations through the inhibition of FAAH can mitigate pain and neuroinflammation (Schlosburg et al., 2009). Several FAAH inhibitors, classified as urea, carbamate, and keto-heterocycle derivatives, have been developed (Seierstad and Breitenbucher, 2008) and progressed to clinical trials to treat inflammatory pain, cannabis dependence, and schizophrenia (Kathuria et al., 2003; Li et al., 2012). Subsequently, to further understand the function of FAAH

[a]Declaration of conflicting interests
The authors declared no potential conflicts of interest with respect to the research, authorship, and/or publication of this article.

https://doi.org/10.1124/jpet.119.263772.
[S] This article has supplemental material available at jpet.aspetjournals.org.

ABBREVIATIONS: BP_{ND}, nondisplaceable binding potential; [^{11}C]CURB, [^{11}C-carbonyl]-6-hydroxy-(1,1'-biphenyl)-3-yl cyclohexylcarbamate; [^{11}C]DFMC, *N*-(3,4-dimethylisoxazol-5-yl)piperazine-4-[4-(2-fluoro-4-[^{11}C]methylphenyl)thiazol-2-yl]-1-carboxamide; %COV, percentage of coefficients of variation[a]; C_P, plasma compartment; FAAH, fatty acid amide hydrolase; ICC, intraclass correlation coefficient; %ID, percent injected dose; MRI, magnetic resonance imaging; PGA, Patlak graphical analysis; PGA_{REF}, PGA reference model; PET, positron emission tomography; SUV, standardized uptake value; TAC, time-activity curve; 1TCM, one-tissue compartment model; 2TCMi, two-tissue compartment model for the irreversible-type radiotracer; URB597, [3-(3-carbamoylphenyl)phenyl] *N*-cyclohexylcarbamate.

and to research drug kinetics in vivo, several positron emission tomography (PET) tracers for FAAH were synthesized based on the inhibitors (Wilson et al., 2011; Rotstein et al., 2014; Kumata et al., 2015; Shimoda et al., 2015, 2016) (Fig. 1).

PET is frequently used as an imaging modality or quantification tool for basic and clinical research to elucidate drug kinetics, molecular density, and distribution in vivo. In general, PET studies with reversible-type radiotracers can acquire the nondisplaceable binding potential (BP_{ND}) as a reasonable index to estimate receptor density (Innis et al., 2007), which permits pharmacological applications, such as the measurement of dose-occupancy relationships for drugs (Saijo et al., 2009). To the best of our knowledge, although two reversible-type PET tracers for FAAH (Fig. 1A) have been developed, both tracers failed to estimate sufficient BP_{ND} values (Liu et al., 2013; Wang et al., 2016). In contrast, PET studies with the irreversible-type radiotracer were generally conducted using two-tissue compartment model analysis with three parameters [$k_4 = 0$, two-tissue compartment model for the irreversible-type radiotracer (2TCMi); Fig. 2]. Of the three parameters, the k_3 consisted of B_{max} multiplied by the association rate constant (k_{on}) to the target molecule. Thus, estimated k_3 gives the most important information for target molecules. Unfortunately, a directly estimated k_3 is usually unstable because of including moderate stochastic varieties. Therefore, the macro parameter [e.g., net uptake value (K_i)] is often estimated as the stable quantitative index for target molecules in place of BP_{ND} value (Egerton et al., 2010; Carter et al., 2012; Rusjan et al., 2013; Frick et al., 2015).

Recently, we have developed *N*-(3,4-dimethylisoxazol-5-yl) piperazine-4-[4-(2-fluoro-4-[^{11}C] methylphenyl)thiazol-2-yl]-1-carboxamide ([^{11}C]DFMC) (Fig. 1B), which has higher affinity for FAAH (IC_{50} = 6.1 nM) than the primary PET tracer [^{11}C-carbonyl]-6-hydroxy-(1,1'-biphenyl)-3-yl cyclohexylcarbamate ([^{11}C]CURB) (IC_{50} = 30 nM). Moreover, [^{11}C]DFMC showed high uptake in rat brain, and the radioactivity was irreversibly trapped (Shimoda et al., 2016).

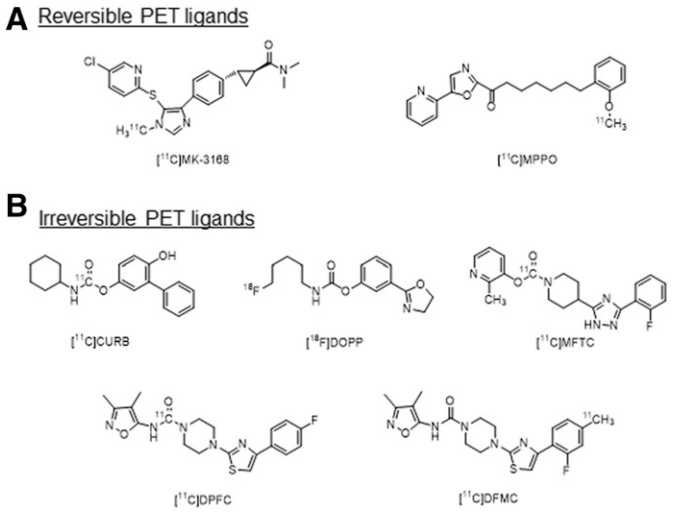

Fig. 1. Current PET tracers for FAAH imaging. (A) Reversible-type PET tracers. (B) Irreversible-type PET tracers.

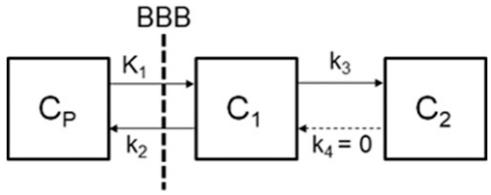

Fig. 2. Schematic of two-tissue compartment model for irreversible-type radiotracer. C_P compartment represents free radiotracer in the plasma. C_1 compartment expresses free and nonspecific binding of radiotracer in brain tissue past the blood-brain barrier (BBB). C_2 compartment displays specific binding of radiotracer with target molecule. K_1 and k_2 describe the influx and efflux rates of radiotracer between C_P and C_1. k_3 and k_4 exhibit the association and dissociation rates of radiotracer to target molecule.

In our study, we first conducted a quantitative PET analysis with blood sampling to estimate the kinetic parameters of [^{11}C]DFMC in various brain regions of the rat. Subsequently, we attempted to noninvasively estimate the net uptake value (K^{REF}) using a reference tissue model and aimed to establish an alternative index for the direct relationship with FAAH concentrations. Finally, to demonstrate the pharmacological utility of PET with [^{11}C]DFMC, we attempted to measure the ED_{50} of [3-(3-carbamoylphenyl)phenyl] *N*-cyclohexylcarbamate (URB597), a clinically used inhibitor of FAAH, using PET with [^{11}C]DFMC in vivo.

Materials and Methods

General

All chemical reagents and organic solvents were purchased from Sigma-Aldrich (St. Louis, MO), FUJIFILM Wako Pure Chem. (Osaka, Japan), or Nacalai Tesque (Kyoto, Japan) and used without further purification. The commercially available compound URB597 (≥98% purity) was purchased from Sigma-Aldrich and dissolved in saline containing 10% ethanol and 5% Tween 20 for animal experiments. ^{11}C was produced using a cyclotron (CYPRIS HM-18; Sumitomo Heavy Industries, Tokyo, Japan). All radioactive values were used with decay correction (a half-life of ^{11}C: 20.4 minutes) (Lederer et al., 1967).

Subjects

Male Sprague-Dawley rats (7–10 weeks old, n = 30) were purchased from Japan SLC (Shizuoka, Japan), housed in a temperature-controlled environment with a 12-hour light/dark cycle, and fed a standard diet. All animal experiments were performed according to the recommendations specified by the Committee for the Care and Use of Laboratory Animals of the National Institutes for Quantum and Radiologic Science and Technology and Animal Research: Reporting of In Vivo Experiments guidelines.

Radiotracer

[^{11}C]DFMC was synthesized according to a previous report (Shimoda et al., 2016). Briefly, [^{11}C]DFMC was synthesized using a C-^{11}C coupling reaction of an aryl boronic ester precursor with [^{11}C]methyl iodide in the presence of a Pd catalyst. Over 370 MBq of [^{11}C]DFMC was obtained with radiochemical purity of >99% and molar activity of >37 GBq/μmol.

PET Study

PET Analysis with Blood Sampling. Prior to the PET scan, a rat (n = 4; 309 ± 14 g) was implanted with a polyethylene catheter (FR2; Imamura, Tokyo, Japan) inserted into the left femoral artery for blood sampling. Subsequently, the rat was secured in a custom-designed chamber and placed in a small-animal PET

scanner (Inveon; Siemens Medical Solutions, Knoxville, TN). Body temperature was maintained using a 40°C water circulation system (T/Pump TP401; Gaymar Industries, Orchard Park, NY). A 24-gauge intravenous catheter (Terumo Medical Products, Tokyo, Japan) was placed into the tail vein of the rat. A bolus of [^{11}C]DFMC (1 ml, 52–57 MBq, 0.3–0.9 nmol) was injected at a flow rate of 0.5 ml/min via a tail vein catheter. Dynamic emission scans in three-dimensional list mode were performed for 90 minutes (10 second × 12 frames, 20 seconds × 3 frames, 30 seconds × 3 frames, 60 seconds × 3 frames, 150 seconds × 3 frames, and 300 seconds × 15 frames). The acquired PET dynamic images were reconstructed by filtered back projection using a Hanning's filter with a Nyquist cutoff of 0.5 cycle/pixel. The time-activity curves (TACs) of [^{11}C]DFMC were acquired from volumes of interest in the cingulate cortex, striatum (caudate/putamen), hippocampus, thalamus, hypothalamus, pons, and cerebellum by referring to a rat brain magnetic resonance imaging (MRI) template using PMOD software (version 3.4; PMOD technology, Zurich, Switzerland). The radioactivity was decay corrected to the injection time and is expressed as the standardized uptake value (SUV).

For the blocking study, a rat (281 g) cannulated as described above was intravenously injected with URB597 at a concentration of 3 mg/kg (0.28 ml vehicle) via the tail vein catheter while under anesthesia. After 30 minutes of anesthesia, a PET assessment with [^{11}C]DFMC (56 MBq; 1.6 nmol) was conducted as described above. volumes of interest were drawn on the spinal cord in addition to general regions.

For counting radioactivity, blood samples were manually collected into microtubes containing heparin (1 μl) at intervals of 20 seconds (0.05 ml for 120 seconds) and 0.5 (0.05 ml for 1 minute), 1 (0.05 ml for 2 minutes), 5 (0.08 ml for 10 minutes), 30 (0.3 ml), 60 (0.4 ml), and 90 minutes (0.5 ml) after initiation of the PET scan. Blood samples were centrifuged at 15,000*g* at 4°C to separate the plasma. The radioactivity in the whole blood and plasma was measured by a 1480 Wizard auto-gamma scintillation counter (PerkinElmer, Waltham, MA). The radioactivity was corrected for decay. For metabolite analysis, six plasma samples were separated at 1 (0.02 ml), 5 (0.02 ml), 15 (0.05 ml), 30 (0.1 ml), 60 (0.2 ml), and 90 minutes (0.3 ml) after the injection.

Metabolite analysis was performed as described previously (Yamasaki et al., 2014). Briefly, whole blood samples were treated to separate the plasma, which was deproteinized with an equivalent amount of acetonitrile. An aliquot of the supernatant obtained from the plasma was analyzed using a high-performance liquid chromatography system with a radiation detector (Takei et al., 2001). Plasma protein binding was not determined in our study. The time curves for a fraction of unchanged [^{11}C]DFMC in the plasma were fitted using three exponential equations and subsequently used for kinetic analyses.

Test-Retest PET Studies. Four rats were used twice within 7 days (285 ± 7 g at first and 323 ± 9 g at the second scan) for PET assessments with [^{11}C]DFMC (47−61 MBq; 0.5−0.8 nmol), and the reliability of the data was assessed using the intraclass correlation coefficient (ICC). The parameters were calculated as follows:

1. Relative difference (%) = (scan 2 − scan 1)/scan 1 × 100
2. Test-retest variability (%) = |scan 2 − scan 1|/[(scan 2 + scan 1)/2] × 100
3. Percentage of coefficients of variation (%COV) = S.D./mean × 100
4. ICC with BSMSS as "mean sum of squares between subjects" and WSMSS as "mean sum of squares within subjects": ICC = (BSMSS − WSMSS)/(BSMSS + WSMSS). An ICC value of −1 denotes no reliability, whereas a value of 1 indicates maximum reliability (Elmenhorst et al., 2012).

Theory

Compartment Model Analysis for Irreversible-Type PET Tracers. To estimate kinetic parameters in PET with [^{11}C]DFMC, 2TCMi (Fig. 2) was conducted. Each rate constant was derived from the following equations:

$$K_1 = FE, \tag{1}$$

$$k_2 = K_1/V_d = FE/V_d, \tag{2}$$

$$k_3 = f_{ND} k_{on} B_{max}, \tag{3}$$

in which K_1 describes the influx rate of radiotracer from the plasma compartment (C_P) to the free and nonspecific compartment (C_1); k_2 represents the efflux rate of radioligand from C_1 to C_P; k_3 describes the transfer from C_1 to the specific-bound compartment (C_2). F is the blood flow, E is the first pass extraction factor, V_d is the distribution volume of the radiotracer in the C_1 compartment, f_{ND} is the tissue-free fraction, k_{on} is the [^{11}C]DFMC-FAAH association rate constant, and B_{max} is the concentration of FAAH. In addition, the K_i as the quantitative index for the net uptake volume of [^{11}C]DFMC with FAAH was determined as follows:

$$K_i = \frac{K_1 k_3}{k_2 + k_3}. \tag{4}$$

To compare the accuracy of K_i values based on $2TCM_i$ (K_i^{2TCMi}), Patlak graphical analysis (PGA) (Patlak et al., 1983) with linear regression was also performed (the slope of a regression line in PGA theoretically equals the K_i value).

A Reference Tissue Model for Irreversible-Type PET Tracers. When reference tissue can be employed, the application of PGA as a reference method [PGA reference model (PGA_{REF})] is possible (Patlak and Blasberg, 1985). In this case, the procedure merely replaces $C_P(t)$ by TAC in the reference tissue. In accordance with a previous report (Patlak and Blasberg, 1985), the slope in graphical analysis reflects the following relation:

$$Slope = K^{REF} = \frac{K_1 k_3}{k_2 + k_3} \times \frac{k_2'}{K_1'\left(1 + K_{eq}'\right)}, \tag{5}$$

in which, K_1', k_2', and K_{eq}' indicate input rate, output rate, and equilibrium constant in the reference area, respectively. In the reference region without irreversible binding, it may be reasonable to assume that $K_{eq}' = 0$ (Patlak and Blasberg, 1985).

Here, $\frac{k_2'}{K_1'}$ is replaced as A,

$$K^{REF} = A\frac{K_1 k_3}{k_2 + k_3} = A \times K_i. \tag{6}$$

Noninvasive Estimation of the Alternative k_3 Value Based on the K^{REF} Value. In this study, we attempted to noninvasively estimate the alternative k_3 (defined as calculated k_3) values, since the K^{REF} value is an indirect index for FAAH concentration. Calculated k_3 is induced by modifying eq. 6.

$$Calculated\ k_3 = \frac{K^{REF} k_2}{AK_1 - K^{REF}} \tag{7}$$

Here, the regional K_1 and k_2 values were fixed by averaged values in 2TCMi analyses (n = 4). The constant A was also displaced as follows:

$$Constant\ A = \frac{K^{REF}}{K_i}. \tag{8}$$

Conditions for the Use of Calculated k_3 Values

In this study, we proposed a calculated k_3 as a new quantitative index for FAAH concentrations. However, there are several conditions for the use of calculated k_3, which are as follows:

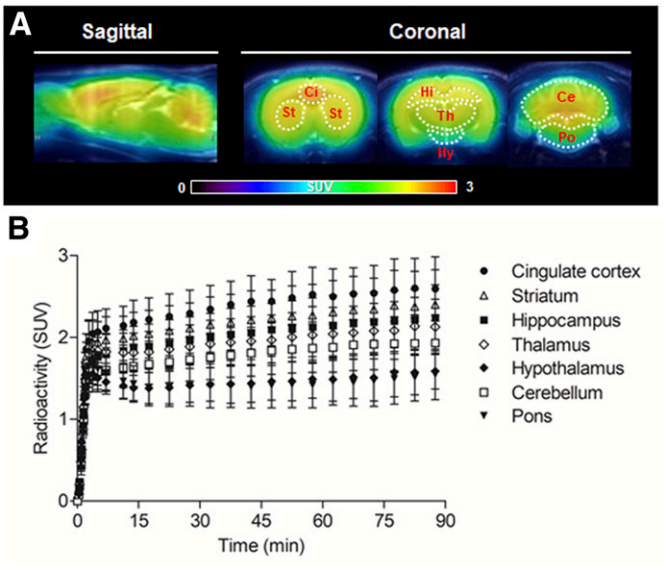

Fig. 3. Representative PET/MRI-fused images (A) and time-activity curves (B) of [^{11}C]DFMC in brain regions (n = 4). PET images were summed between 0 to 90 minutes of acquisition data. The radioactivity was expressed by SUV. Ce, cerebellum; Ci, cingulate cortex; Hi, hippocampus; Hy, hypothalamus; Po, pons; St, striatum; Th, thalamus.

1. To estimate averaged K_1, k_2, and constant A, several repeated PET assessments with blood sampling and compartment model analyses are essential in advance of these estimates.
2. It is required that there are no differences in influx (K_1) and efflux (k_2) rates of radiotracer between the research subject and the baseline subject.
3. The calculated k_3 remains an unstable value and therefore includes a specific variation based on individual differences. To surmount this disadvantage, several samples sizes ($n \geq 3$, at least) should be considered.

Although there are several limitations, it would be valuable to consider whether calculated k_3 can be adapted because calculated k_3 in multidose response assays using PET could be more easily obtained than direct k_3 with blood sampling.

Multidose URB597 Treatment-Response Assays

A series of dynamic PET scans ([^{11}C]DFMC: 38–60 MBq; 0.3–1.0 nmol) without blood sampling were performed for each rat (n = 3 for each dose; 241–319 g) 30 minutes after administration with different doses of URB597 (0.003, 0.01, 0.03, 0.1, 0.3, 1, and 3 mg/kg in 0.3-ml vehicle).

The results of the inhibitory experiments were subjected to nonlinear regression analysis using Prism 5 (GraphPad Software, La Jolla, CA), and ED_{50} values of URB597 were calculated using each averaged calculated k_3 value of several brain regions (cingulate cortex, striatum, hippocampus, thalamus, and cerebellum).

Statistical Methods

Goodness of fit was evaluated using the Akaike information criterion (Akaike, 1974) and the model selection criterion (Handbook, 1995). Values are given as mean ± S.D. The %COV was estimated from the diagonal of the covariance matrix of the fitting. All data analyses were performed using GraphPad Prism v5.0 (GraphPad Software).

Results

Invasive Quantitative PET Analysis Using [^{11}C]DFMC. Figure 3 show representative averaged PET/MRI images (A) and TACs (B) in brain regions. High uptake of radioactivity was detected in the cingulate cortex and striatum (caudate/putamen), and moderate radioactivity was detected in the hippocampus, thalamus, cerebral cortex, and cerebellum. Meanwhile, radioactivity in the hypothalamus and pons was relatively low. These radioactive distribution patterns corresponded with the distribution of FAAH concentrations (Thomas, et al., 1997). TACs in FAAH-rich brain regions constantly increased without clearance after the injection of [^{11}C]DFMC.

Figure 4A shows the metabolite-corrected plasma input function of [^{11}C]DFMC. The unchanged [^{11}C]DFMC in the arterial plasma peaked at 4.19 ± 0.72 SUV 2 minutes after the injection and declined to 0.35 ± 0.03 SUV 5 minutes after the injection and 0.04 ± 0.01 SUV 90 minutes after the injection. The metabolic rate of [^{11}C]DFMC was relatively slow: >65% of the parent compound remained 30 minutes after the injection, and roughly 30% of the parent compound remained 90 minutes after the injection.

Figure 4B shows TACs with a one-tissue compartment model (1TCM) containing C_P and C_1 compartments only, and 2TCMi fitting curves in the cingulate cortex. The 1TCM showed a poorly fitting curve for TACs. Conversely, the fitting curve for 2TCMi showed a good shape and indicated good scores (see Supplemental Table 1) regarding the goodness of fit. Thus, the 2TCMi is an adequate kinetic model for this radiotracer. Detailed full kinetic parameters in brain regions are shown in Table 1. Of the rate constants, the directly estimated k_3 values were acquired as 0.08–0.18 minutes^{-1}

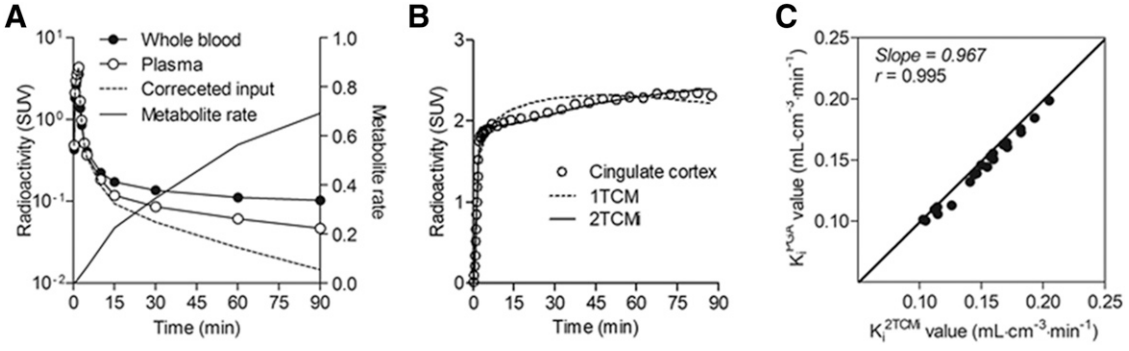

Fig. 4. Curve-fitting analysis using input function in PET with [^{11}C]DFMC. (A) Plasma input curves of [^{11}C]DFMC. (B) Comparison between 1TCM and 2TCMi curve fittings of data from the cingulate cortex. (C) Correlation plots between K_i values based on 2TCMi and K_i values based on PGA in rat brains (n = 4).

TABLE 1
Kinetic rate constants estimated with 2TCMi in PET with [^{11}C]DFMC (n = 4, mean ± S.D.) The %COV was expressed within parentheses.

Regions	K_1 (ml·cm^{-3}·min^{-1})	k_2 (min^{-1})	k_3 (min^{-1})	K_1/k_2 (ml·cm^{-3})	λk_3 (ml·cm^{-3}·min^{-1})	K_i (ml·cm^{-3}·min^{-1})	Patlak K_i (ml·cm^{-3}·min^{-1})
Cingulate cortex	0.32 ± 0.06	0.09 ± 0.03	0.18 ± 0.04	3.62 ± 0.69	0.62 ± 0.12	0.21 ± 0.04	0.21 ± 0.04
	(1.4 ± 0.1)	(12.9 ± 2.3)	(9.5 ± 2.2)	(11.4 ± 2.2)	(15.9 ± 3.2)	(0.0 ± 0.1)	(0.8 ± 0.1)
Striatum	0.31 ± 0.06	0.10 ± 0.02	0.16 ± 0.03	3.37 ± 0.75	0.53 ± 0.17	0.20 ± 0.04	0.19 ± 0.05
	(1.4 ± 0.2)	(9.7 ± 1.5)	(7.2 ± 1.3)	(8.5 ± 1.4)	(15.6 ± 2.7)	(0.2 ± 0.2)	(0.5 ± 0.1)
Hippocampus	0.27 ± 0.05	0.08 ± 0.03	0.16 ± 0.04	3.49 ± 0.88	0.56 ± 0.18	0.18 ± 0.04	0.18 ± 0.04
	(1.1 ± 0.1)	(9.0 ± 1.5)	(6.7 ± 1.4)	(8.0 ± 1.5)	(14.7 ± 2.9)	(0.0 ± 0.2)	(0.4 ± 0.1)
Thalamus	0.30 ± 0.05	0.10 ± 0.02	0.13 ± 0.02	3.11 ± 0.46	0.42 ± 0.12	0.17 ± 0.04	0.17 ± 0.04
	(1.2 ± 0.2)	(7.3 ± 1.7)	(5.5 ± 1.4)	(6.3 ± 1.5)	(11.8 ± 2.9)	(0.3 ± 0.1)	(0.7 ± 0.2)
Hypothalamus	0.27 ± 0.04	0.13 ± 0.01	0.12 ± 0.02	2.07 ± 0.20	0.25 ± 0.07	0.13 ± 0.03	0.12 ± 0.03
	(1.8 ± 0.3)	(8.5 ± 1.9)	(6.5 ± 1.5)	(7.0 ± 1.6)	(13.5 ± 3.1)	(0.8 ± 0.2)	(1.8 ± 0.7)
Cerebellum	0.26 ± 0.05	0.11 ± 0.03	0.16 ± 0.03	2.58 ± 0.63	0.42 ± 0.11	0.16 ± 0.03	0.15 ± 0.03
	(1.4 ± 0.1)	(8.9 ± 1.3)	(6.6 ± 1.3)	(7.8 ± 1.3)	(14.4 ± 2.5)	(0.1 ± 0.1)	(0.5 ± 0.3)
Pons	0.28 ± 0.04	0.11 ± 0.01	0.08 ± 0.01	2.58 ± 0.54	0.22 ± 0.08	0.12 ± 0.03	0.12 ± 0.03
	(1.2 ± 0.2)	(5.6 ± 1.2)	(4.6 ± 1.5)	(4.6 ± 1.0)	(9.3 ± 2.0)	(0.7 ± 0.2)	(1.3 ± 0.9)

with 4.6%–9.5%COV in the regions of interest. The macroparameter K_i values for the quantitative uptake value of [^{11}C]DFMC were obtained as 0.12–0.21 ml·cm^{-3}·min^{-1} with 0.0%–0.8%COV in the investigated brain regions.

Next, to validate the accuracy of the estimated K_i values based on the compartmental analysis (K_i^{2TCMi}), we compared these values with those based on graphical analysis (K_i^{PGA}), as shown in Fig. 4C. The slope of the resulting regression line was almost 1 (0.967) and the r-value was 0.995. These results indicate a high correlation between K_i^{PGA} and K_i^{2TCMi} values, which suggests that K_i^{2TCMi} values were estimated with high reliability.

Validation Studies for the PGA Reference Model. Figure 5, A and B show representative PET-averaged images (A) and TACs (B) in the cingulate cortex and spinal cord of rats pretreated with or without URB597 (3 mg/kg). Radioactivity in the cingulate cortex of the baseline subject was accumulated at a high level without clearance during the PET scan, which was significantly decreased by pretreatment with URB597. Meanwhile, uptake of radioactivity between the baseline and blocking subjects showed no significant differences (P = 0.106) in the spinal cord (Fig. 5B), which suggests that the spinal cord adequately serves as the reference region.

Subsequently, to noninvasively estimate net uptake values (defined as K^{REF}), we performed the PGA_{REF} using the TAC of the spinal cord as a reference region. The validity of K^{REF} values was evaluated by comparing with K_i^{2TCMi} values. Figure 5C shows the relationship between the averaged K^{REF} and K_i^{2TCMi} values in baseline subjects (n = 4). The slope (k_2'/K_1', defined as constant A, see eq. 8) of the regression line was 0.075 with high correlation (r = 0.981, $P < 0.001$) and a small intercept (−0.004).

Additionally, to support the accuracy of K^{REF} estimations, the reproducibility of the K^{REF} values was evaluated by a test-retest study using PET with [^{11}C]DFMC. Table 2 shows the reproducibility of the test-retest PET study for the estimation of K^{REF}. In the cingulate cortex, the FAAH-richest region in the brain, the percentage of variability, ICC, and Pearson's r were 8.8, 0.836, and 0.900, respectively. Additionally, the correlation (Pearson's r) between test and retest outcomes in all regions of interest was 0.891, indicating high reproducibility of K^{REF} values after PET with [^{11}C]DFMC.

Estimation for Calculated k_3 Values. The K^{REF} value is an indirect index of FAAH concentration due to the macroparameter containing K_1, k_2, and k_3 rate constants. We attempted to noninvasively estimate an alternative k_3 value (defined as calculated k_3) by inserting measured K^{REF} values, constant A, and fixed values (averaged K_1 and k_2 values in 2TCMi). Here, because K^{REF} values included a small bias (−0.004) compared with K_i^{2TCMi} values as described above (Fig. 5C), we modified eq. 7 as follows:

$$Calculated\ k_3 = \frac{(K^{REF} - bias)k_2}{AK_1 - (K^{REF} - bias)}. \quad (9)$$

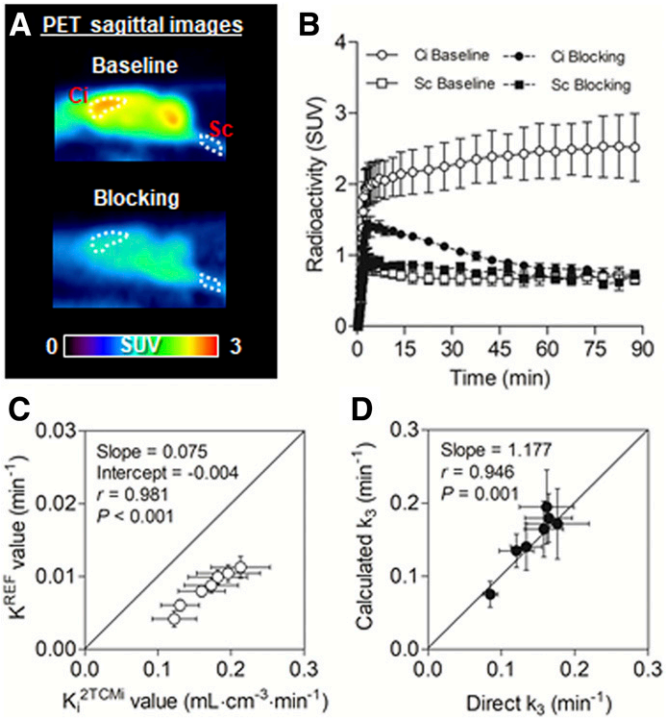

Fig. 5. Validation study for the use of the reference model. (A) Representative PET images of the baseline (top) and blocking (bottom, pretreatment with URB597 of 3 mg/kg) rats. (B) Time-activity curves of [^{11}C]DFMC in the cingulate cortex (Ci) and spinal cord (Sc) of the baseline (n = 4) and blocking (n = 3) rats. (C) Correlation plots between averaged K^{REF} value based on PGA_{REF} and the averaged K_i value based on 2TCMi in rat brains (n = 4). (D) The relationship between an averaged calculated k_3 value (estimating from measured K^{REF}, constant A, averaged K_1, k_2, and the bias of reference region) and averaged direct k_3 values in the compartment model analysis.

TABLE 2
Reliability of outcome parameters in test-retest PET studies with [^{11}C]DFMC (n = 4)

Region	K^{REF} value (min^{-1})		Relative Difference (%) (Mean ± S.D.)	%Variability (Mean ± S.D.)	ICC	Pearson's r
	Test (Mean ± S.D.)	Retest (Mean ± S.D.)				
Cingulate cortex	0.0108 ± 0.0021	0.0100 ± 0.0026	−7.3 ± 10.3	8.8 ± 10.8	0.836	0.900
Striatum	0.0092 ± 0.0027	0.0093 ± 0.0017	5.3 ± 21.4	11.8 ± 13.6	0.835	0.909
Hippocampus	0.0098 ± 0.0025	0.0095 ± 0.0011	1.3 ± 22.5	15.0 ± 10.9	0.681	0.892
Thalamus	0.0081 ± 0.0023	0.0077 ± 0.0009	−1.5 ± 20.0	14.8 ± 9.1	0.700	0.976
Hypothalamus	0.0045 ± 0.0018	0.0041 ± 0.0016	7.8 ± 76.8	47.2 ± 36.3	0.430	0.226
Cerebellum	0.0080 ± 0.0024	0.0078 ± 0.0014	2.9 ± 24.9	15.3 ± 14.4	0.735	0.795
Pons	0.0040 ± 0.0015	0.0030 ± 0.0011	−18.8 ± 41.7	45.5 ± 23.7	0.369	0.304

Figure 5D exhibits the relationship between averaged calculated k_3 and the directly estimated k_3 values. Although both k_3 values were robust, the slope of the regression line was 1.177 and showed high correlation (r = 0.946, P = 0.001). This result suggested that the calculated k_3 value would be useful as a direct index of FAAH concentration.

Estimation for ED_{50} of URB597 Using Calculated k_3. Figure 6 shows representative PET/MRI images (A) of rat brains treated with multiple doses of URB597 and dose responses of calculated k_3 values (B) in the cingulate cortex, striatum, hippocampus, thalamus, and cerebellum. Radioactivity in all brain regions was gradually decreased by increasing the URB597 doses (Fig. 6A). Treatment with 1 mg/kg URB597 almost completely blocked the accumulation of radioactivity in the brain, and the calculated k_3 was close to zero. Thus, the ED_{50} value for URB597 was estimated to be 66.4 μg/kg in rat brain (Fig. 6B).

Discussion

In our study, [^{11}C]DFMC, the most recently developed PET tracer for FAAH imaging, was used for the index measurement reflecting FAAH concentrations in the brain. The first quantitative PET study for FAAH was performed using [^{11}C]CURB, a primary PET tracer for FAAH. In that report, the rate constant k_3 for [^{11}C]CURB in PET with 2TCMi analysis was under 0.06 $minutes^{-1}$ in the human brain (Rusjan et al., 2013). 6-Hydroxy-[1,1'-biphenyl]-3-yl cyclohexylcarbamate is a URB597 derivative and has lower affinity (IC_{50} = 30 nM) for FAAH than URB597 (IC_{50} = 7.7 nM) (Clapper et al., 2009). *N*-(3,4-Dimethylisoxazol-5-yl)-4-(4-(2-fluoro-4-methylphenyl) thiazol-2-yl)piperazine-1-carboxamide has been recently developed as an inhibitor possessing a 3-fold higher affinity for FAAH than URB597 (Shimoda et al., 2016). Although the study subjects were different in this study, FAAH between the human and the rat is known to have high biologic homology and similar V_{max} values in brains (Desarnaud et al., 1995; Giang and Cravatt, 1997; Maccarrone et al., 1998). Therefore, an estimated k_3 with over 0.1 $minutes^{-1}$ in every FAAH-rich region of rat brain in the compartmental analysis of [^{11}C]DFMC (Table 1) would reflect a high affinity for FAAH, as described in eq. 3. Thus, [^{11}C]DFMC showing a much k_3 value would be a reasonable radiotracer for PET assessments.

To promote applications using PET with [^{11}C]DFMC, we tried to noninvasively estimate the macroparameter K_i value, including k_3, using the reference tissue method. Prior to kinetic analysis, a blocking PET study using URB597 (3 mg/kg) was conducted to determine the reference region. The heterogeneous uptake of radioactivity in all brain regions of control subjects showed significant displaceability by pretreatment with URB597, whereas radioactive uptake in the spinal cord exhibited nondisplaceable uptake (Fig. 5). In a pathologic report, FAAH-containing neurons were detected in the cerebral cortex, hippocampus, and Purkinje cells of the cerebellar cortex but not in the spinal cord (Tsou et al., 1998). However, to our knowledge, there are no reports regarding quantitative PET analysis using the spinal cord as a reference region. Therefore, we performed a test-retest PET study to validate the use of the spinal cord as a reference region. The ICC of the K^{REF} value in FAAH-rich regions was 0.681–0.836 (Table 2), which supported relatively high reliability for K^{REF} values in the PET study using [^{11}C]DFMC with PGA_{REF}. Meanwhile, a high variability (>40%) was detected in the low-FAAH regions ($K^{REF} < 0.005$ $minutes^{-1}$), such as the hypothalamus and pons. The K^{REF} value was concisely estimated with high reproducibility in FAAH-rich regions.

Another concern is the differences in distribution volumes (K_1/k_2) between the region of interest and the reference region. Theoretically, the K^{REF} value equals $k_2k_3/(k_2+k_3)$ in the case of $K_1/k_2 = K_1'/k_2'$ (see eq. 5). However, in this study, the distribution

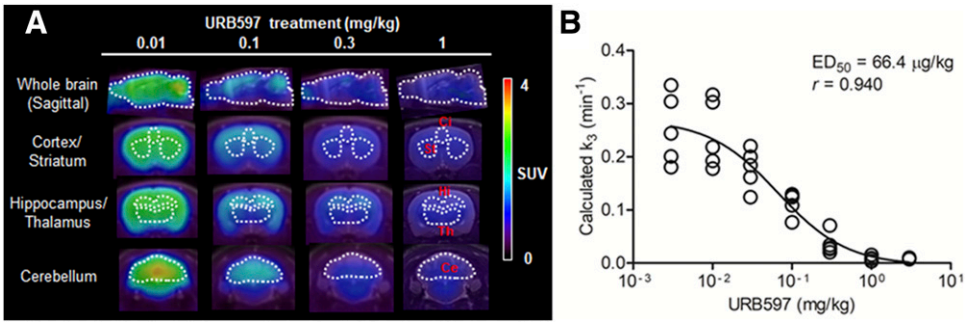

Fig. 6. Dose-response assay using URB597. (A) Representative PET/MRI images of [^{11}C]DFMC in the brains of rats treated with different doses (0.01, 0.1, 0.3, and 1 mg/kg) of URB597. (B) The relationship between calculated k_3 values ($minute^{-1}$) and doses of URB597 in various brain regions. Averaged values of calculated k_3 in the cingulate cortex, striatum, hippocampus, thalamus, and cerebellum are plotted against the dose of URB597. Ce, cerebellum; Ci, cingulate cortex; Hi, hippocampus; St, striatum; Th, thalamus.

volume in the spinal cord (K_1'/k_2') did not equal K_1/k_2 in other brain regions (see in Supplemental Table 2). Therefore, the K^{REF} values are modified to $K_1k_3/(k_2+k_3)(k_2'/K_1')$. In the results of the PGA_{REF} analysis, the K^{REF} values in brain regions were estimated with a range of 0.004–0.011 minutes^{-1}. Compared with the K_i^{2TCMi} values, the K^{REF} values showed high correlation ($r > 0.95$; Fig. 5C). In this regression, the slope showed 0.075 (= k_2'/K_1'), which is defined as constant A in eq. 8. However, a small negative bias (−0.004) of the K^{REF} value was recognized, although PGA_{REF} and K_i^{2TCMi} are proportional in theory. This small negative bias may be caused by the slight accumulation of the radiotracer at nondisplaceable sites in the spinal cord, which would cause an undesirable increase in the value of TAC in the spinal cord. Nevertheless, the spinal cord would be an adequate reference region for the estimation of regional K^{REF} values in the present PGA_{REF} analysis. Moreover, estimated K^{REF} values would be a reasonable index for alternative net uptake values of [^{11}C]DFMC with FAAH despite including a small bias.

Finally, to propose a pharmacological application of [^{11}C]DFMC-PET using K^{REF} values, we estimated ED_{50} values of URB597 in the brain in vivo. URB597 has been developed a decade before (Fegley et al., 2005), and widely tested as a treatment of neuroinflammation and pain (Murphy et al., 2012; Lomazzo et al., 2015). Here, since the K^{REF} value is not proportional to the regional FAAH concentrations in theory (eqs. 3 and 6), we tentatively estimated the k_3 value (defined as calculated k_3) from K^{REF} value (eq. 9). In a comparison of the directly estimated k_3 obtained by the compartmental analysis with blood sampling, the calculated k_3 showed high correlation ($r = 0.946$), although a slight overestimation was exhibited (Fig. 5D). This result suggested that the calculated k_3 would be favorably used as an alternative parameter of the directly estimated k_3 value, which motivated us to progress our pharmacological application study. However, there is a considerable limitation in the use of calculated k_3. Since the equation for calculated k_3 includes two variable parameters, K_1 and k_2, it is important that administration of URB597 does not affect blood flow. Fortunately, administration of under 1 mg/kg (the maximum dose used in this assessment) of URB597 did not produce any effects on the initial uptake of radioactivity (Supplemental Fig. 1). Therefore, the present dose-response assay using the calculated k_3 would be expected to give reasonable ED_{50} values of URB597 in brain regions without effects on blood flow.

Although the assay used a calculated-k_3, the ED_{50} values of URB597 were estimated to be 66.4 μg/kg (0.2 μmol/kg ≈ 60 nmol/head) in the rat brain (Fig. 6B). Previously, we reported that the in vitro IC_{50} value of URB597 using a membrane fraction of rat brain was 19.6 ± 3.5 nM (Shimoda et al., 2016). It was previously reported that an ^{11}C-labeled URB597 analog remained at 0.6 percentage of injection dose per gram tissue (%ID/g) in the brain of mice 60 minutes after injection (Wyffels et al., 2010). In general, the %ID/g value of rat brain is roughly 10-fold lower than that of the mouse brain because of the differences in body weights. Therefore, the present ED_{50} value of URB597 was supposed to be approximately 36 pmol/g brain ([injection dose of URB597 (60 nmol/head)] × 0.06%ID/g brain) in PET with [^{11}C]DFMC. The present in vivo ED_{50} value (36 nmol/kg brain) could be concisely estimated since it was close to the in vitro measurement (19.6 nmol/l).

In summary, we demonstrated the noninvasive estimation of the K^{REF} value of [^{11}C]DFMC in FAAH-containing brain regions using the reference tissue model. Moreover, by using K^{REF} value, we proposed calculated k_3 as an alternative index for the quantification of FAAH. Finally, using calculated k_3, we estimated ED_{50} value of URB597 responsible for FAAH inhibition in rat brain as one of the pharmacological applications in vivo. Thus, our technique using PET with [^{11}C]DFMC could contribute to occupancy studies using rats for new pharmaceuticals for the treatment of central nervous system disorders targeting FAAH.

Acknowledgments

We thank the staff of the National Institute of Radiological Sciences for their support with the following: cyclotron operation, radioisotope production, radiosynthesis, and animal experiments. We thank Trent Rogers from Edanz Group (www.edanzediting.com/ac) for editing a draft of this manuscript.

Authorship Contributions

Participated in research design: Yamasaki T, Ohya T.

Conducted experiments: Yamasaki T, Zhang Y, Wakizaka H.

Contributed new reagents or analytic tools: Mori W, Nengaki N, Fujinaga M.

Performed data analysis: Yamasaki T.

Wrote or contributed to the writing of the manuscript: Yamasaki T, Ohya T, Kikuchi T, Zhang MR.

References

Ahn K, McKinney MK, and Cravatt BF (2008) Enzymatic pathways that regulate endocannabinoid signaling in the nervous system. *Chem Rev* **108**:1687–1707.

Akaike H (1974) A new look at the statistical model identification. *IEEE Trans Auto Cont* **19**:716–723.

Bayewitch M, Avidor-Reiss T, Levy R, Barg J, Mechoulam R, and Vogel Z (1995) The peripheral cannabinoid receptor: adenylate cyclase inhibition and G protein coupling. *FEBS Lett* **375**:143–147.

Carter SF, Schöll M, Almkvist O, Wall A, Engler H, Långström B, and Nordberg A (2012) Evidence for astrocytosis in prodromal Alzheimer disease provided by 11C-deuterium-L-deprenyl: a multitracer PET paradigm combining 11C-Pittsburgh compound B and 18F-FDG. *J Nucl Med* **53**:37–46.

Clapper JR, Vacondio F, King AR, Duranti A, Tontini A, Silva C, Sanchini S, Tarzia G, Mor M, and Piomelli D (2009) A second generation of carbamate-based fatty acid amide hydrolase inhibitors with improved activity in vivo. *ChemMedChem* **4**:1505–1513.

Desarnaud F, Cadas H, and Piomelli D (1995) Anandamide amidohydrolase activity in rat brain microsomes. Identification and partial characterization. *J Biol Chem* **270**:6030–6035.

Devane WA, Hanus L, Breuer A, Pertwee RG, Stevenson LA, Griffin G, Gibson D, Mandelbaum A, Etinger A, and Mechoulam R (1992) Isolation and structure of a brain constituent that binds to the cannabinoid receptor. *Science* **258**: 1946–1949.

Egerton A, Demjaha A, McGuire P, Mehta MA, and Howes OD (2010) The test-retest reliability of 18F-DOPA PET in assessing striatal and extrastriatal presynaptic dopaminergic function. *Neuroimage* **50**:524–531.

Elmenhorst D, Aliaga A, Bauer A, and Rosa-Neto P (2012) Test-retest stability of cerebral $mGluR_5$ quantification using [^{11}C]ABP688 and positron emission tomography in rats. *Synapse* **66**:552–560.

Fegley D, Gaetani S, Duranti A, Tontini A, Mor M, Tarzia G, and Piomelli D (2005) Characterization of the fatty acid amide hydrolase inhibitor cyclohexyl carbamic acid 3′-carbamoyl-biphenyl-3-yl ester (URB597): effects on anandamide and oleoylethanolamide deactivation. *J Pharmacol Exp Ther* **313**: 352–358.

Frick A, Ahs F, Linnman C, Jonasson M, Appel L, Lubberink M, Långström B, Fredrikson M, and Furmark T (2015) Increased neurokinin-1 receptor availability in the amygdala in social anxiety disorder: a positron emission tomography study with [11C]GR205171. *Transl Psychiatry* **5**:e597.

Giang DK and Cravatt BF (1997) Molecular characterization of human and mouse fatty acid amide hydrolases. *Proc Natl Acad Sci USA* **94**:2238–2242.

Handbook MS (1995) *Rev., 7EEF*. p 467, MicroMath, Inc., Salt Lake City, UT.

Innis RB, Cunningham VJ, Delforge J, Fujita M, Gjedde A, Gunn RN, Holden J, Houle S, Huang SC, Ichise M, et al. (2007) Consensus nomenclature for in vivo imaging of reversibly binding radioligands. *J Cereb Blood Flow Metab* **27**: 1533–1539.

Kathuria S, Gaetani S, Fegley D, Valiño F, Duranti A, Tontini A, Mor M, Tarzia G, La Rana G, Calignano A, et al. (2003) Modulation of anxiety through blockade of anandamide hydrolysis. *Nat Med* **9**:76–81.

Kumata K, Yui J, Hatori A, Maeda J, Xie L, Ogawa M, Yamasaki T, Nagai Y, Shimoda Y, Fujinaga M, et al. (2015) Development of [(11)C]MFTC for PET imaging of

fatty acid amide hydrolase in rat and monkey brains. *ACS Chem Neurosci* **6**: 339–346.
Lederer CM, Hollander JM, and Perlman I (1967) *Table of Isotopes*, 6th ed. Wiley, New York.
Li GL, Winter H, Arends R, Jay GW, Le V, Young T, and Huggins JP (2012) Assessment of the pharmacology and tolerability of PF-04457845, an irreversible inhibitor of fatty acid amide hydrolase-1, in healthy subjects. *Br J Clin Pharmacol* **73**:706–716.
Liu P, Hamill TG, Chioda M, Chobanian H, Fung S, Guo Y, Chang L, Bakshi R, Hong Q, Dellureficio J, et al. (2013) Discovery of MK-3168: a PET tracer for imaging brain fatty acid amide hydrolase. *ACS Med Chem Lett* **4**:509–513.
Lomazzo E, Bindila L, Remmers F, Lerner R, Schwitter C, Hoheisel U, and Lutz B (2015) Therapeutic potential of inhibitors of endocannabinoid degradation for the treatment of stress-related hyperalgesia in an animal model of chronic pain. *Neuropsychopharmacology* **40**:488–501.
Maccarrone M, van der Stelt M, Rossi A, Veldink GA, Vliegenthart JF, and Agrò AF (1998) Anandamide hydrolysis by human cells in culture and brain. *J Biol Chem* **273**:32332–32339.
Malek N, Popiolek-Barczyk K, Mika J, Przewlocka B, and Starowicz K (2015) Anandamide, acting via CB2 receptors, alleviates LPS-induced neuroinflammation in rat primary microglial cultures. *Neural Plast* **2015**:130639.
Murphy N, Cowley TR, Blau CW, Dempsey CN, Noonan J, Gowran A, Tanveer R, Olango WM, Finn DP, Campbell VA, et al. (2012) The fatty acid amide hydrolase inhibitor URB597 exerts anti-inflammatory effects in hippocampus of aged rats and restores an age-related deficit in long-term potentiation. *J Neuroinflammation* **9**:79.
Pacher P, Bátkai S, and Kunos G (2006) The endocannabinoid system as an emerging target of pharmacotherapy. *Pharmacol Rev* **58**:389–462.
Patlak CS and Blasberg RG (1985) Graphical evaluation of blood-to-brain transfer constants from multiple-time uptake data. Generalizations. *J Cereb Blood Flow Metab* **5**:584–590.
Patlak CS, Blasberg RG, and Fenstermacher JD (1983) Graphical evaluation of blood-to-brain transfer constants from multiple-time uptake data. *J Cereb Blood Flow Metab* **3**:1–7.
Piomelli D (2003) The molecular logic of endocannabinoid signalling. *Nat Rev Neurosci* **4**:873–884.
Raboune S, Stuart JM, Leishman E, Takacs SM, Rhodes B, Basnet A, Jameyfield E, McHugh D, Widlanski T, and Bradshaw HB (2014) Novel endogenous N-acyl amides activate TRPV1-4 receptors, BV-2 microglia, and are regulated in brain in an acute model of inflammation. *Front Cell Neurosci* **8**:195.
Rotstein BH, Wey HY, Shoup TM, Wilson AA, Liang SH, Hooker JM, and Vasdev N (2014) PET imaging of fatty acid amide hydrolase with [(18)F]DOPP in nonhuman primates. *Mol Pharm* **11**:3832–3838.
Rusjan PM, Wilson AA, Mizrahi R, Boileau I, Chavez SE, Lobaugh NJ, Kish SJ, Houle S, and Tong J (2013) Mapping human brain fatty acid amide hydrolase activity with PET. *J Cereb Blood Flow Metab* **33**:407–414.
Saijo T, Maeda J, Okauchi T, Maeda J, Morio Y, Kuwahara Y, Suzuki M, Goto N, Suzuki K, Higuchi M, et al. (2009) Utility of small-animal positron emission tomographic imaging of rats for preclinical development of drugs acting on the serotonin transporter. *Int J Neuropsychopharmacol* **12**:1021–1032.
Schlosburg JE, Kinsey SG, and Lichtman AH (2009) Targeting fatty acid amide hydrolase (FAAH) to treat pain and inflammation. *AAPS J* **11**:39–44.
Seierstad M and Breitenbucher JG (2008) Discovery and development of fatty acid amide hydrolase (FAAH) inhibitors. *J Med Chem* **51**:7327–7343.
Shimoda Y, Fujinaga M, Hatori A, Yui J, Zhang Y, Nengaki N, Kurihara Y, Yamasaki T, Xie L, Kumata K, et al. (2016) N-(3,4-Dimethylisoxazol-5-yl)piperazine-4-[4-(2-fluoro-4-[(11)C] methylphenyl)thiazol-2-yl]-1-carboxamide: a promising positron emission tomography ligand for fatty acid amide hydrolase. *Bioorg Med Chem* **24**:627–634.
Shimoda Y, Yui J, Zhang Y, Hatori A, Ogawa M, Fujinaga M, Yamasaki T, Xie L, Kumata K, and Zhang MR (2015) Radiosynthesis and evaluation of N-(3,4-dimethylisoxazol-5-yl)piperazine-4-[4-(4-fluorophenyl) thiazol-2-yl]-1-[C-11] carboxamide for in vivo positron emission tomography imaging of fatty acid amide hydrolase in brain. *RSC Adv* **5**:106122–106127.
Takei M, Kida T, and Suzuki K (2001) Sensitive measurement of positron emitters eluted from HPLC. *Appl Radiat Isot* **55**:229–234.
Thomas EA, Cravatt BF, Danielson PE, Gilula NB, and Sutcliffe JG (1997) Fatty acid amide hydrolase, the degradative enzyme for anandamide and oleamide, has selective distribution in neurons within the rat central nervous system. *J Neurosci Res* **50**:1047–1052.
Tsou K, Nogueron MI, Muthian S, Sañudo-Pena MC, Hillard CJ, Deutsch DG, and Walker JM (1998) Fatty acid amide hydrolase is located preferentially in large neurons in the rat central nervous system as revealed by immunohistochemistry. *Neurosci Lett* **254**:137–140.
Wang L, Yui J, Wang Q, Zhang Y, Mori W, Shimoda Y, Fujinaga M, Kumata K, Yamasaki T, Hatori A, et al. (2016) Synthesis and preliminary PET imaging studies of a FAAH radiotracer ([11C]MPPO) based on α-ketoheterocyclic scaffold. *ACS Chem Neurosci* **7**:109–118.
Wilson AA, Garcia A, Parkes J, Houle S, Tong J, and Vasdev N (2011) [11C]CURB: evaluation of a novel radiotracer for imaging fatty acid amide hydrolase by positron emission tomography. *Nucl Med Biol* **38**:247–253.
Wyffels L, Muccioli GG, Kapanda CN, Labar G, De Bruyne S, De Vos F, and Lambert DM (2010) PET imaging of fatty acid amide hydrolase in the brain: synthesis and biological evaluation of an 11C-labelled URB597 analogue. *Nucl Med Biol* **37**: 665–675.
Yamasaki T, Fujinaga M, Yui J, Ikoma Y, Hatori A, Xie L, Wakizaka H, Kumata K, Nengaki N, Kawamura K, et al. (2014) Noninvasive quantification of metabotropic glutamate receptor type 1 with [^{11}C]ITDM: a small-animal PET study. *J Cereb Blood Flow Metab* **34**:606–612.

Address correspondence to: Dr. Tomoteru Yamasaki, Department of Advanced Nuclear Medicine Sciences, National Institute of Radiological Sciences, Quantum Medical Science Directorate, National Institutes for Quantum and Radiological Science and Technology, 4-9-1 Anagawa, Inage-ku, Chiba 263-8555, Japan. E-mail: yamasaki.tomoteru@qst.go.jp